Mud volcano response to the 4 April 2010 El Mayor-Cucapah earthquake

M. L. Rudolph[1] and M. Manga[1]

Received 28 May 2010; revised 18 August 2010; accepted 4 October 2010; published 31 December 2010.

[1] Mud volcanoes sometimes respond to earthquakes, but the mechanisms by which earthquakes trigger changes in ongoing eruptions or initiate new eruptions are not completely understood. We measured gas discharge at a field of mud volcanoes near the Salton Sea, southern California, before and after the 4 April 2010 El Mayor-Cucapah earthquake and observed an increase in gas flux immediately following the earthquake and a subsequent recovery to pre-earthquake values. This earthquake-eruption pair is of particular interest because the earthquake produced large strains, up to 1.2%, near the mud volcano location, allowing us to test two competing triggering mechanisms: (1) shaking-induced bubble mobilization and (2) permeability enhancement. We measured the rheology of erupted mud from the mud volcanoes to quantify the importance of mechanism 1 and found that this mechanism is unlikely to be important. We therefore favor the explanation that the increased gas flux was caused by a transient increase in permeability.

Citation: Rudolph, M. L., and M. Manga (2010), Mud volcano response to the 4 April 2010 El Mayor-Cucapah earthquake, *J. Geophys. Res.*, *115*, B12211, doi:10.1029/2010JB007737.

1. Introduction

[2] Earthquakes induce a wide range of hydrologic responses including water level changes in wells, changes in spring discharge and stream flow [e.g., *Muir-Wood and King*, 1993], changes in permeability [e.g., *Elkhoury et al.*, 2006], and changes in the interval between eruptions of geysers [e.g., *Husen et al.*, 2004]. Mud volcanoes also respond to earthquakes [e.g., *Mellors et al.*, 2007], and their responses may have hydrologic origins. Although hydrologic responses to earthquakes have been well documented for thousands of years, the mechanisms responsible for the responses and their possible relationship to triggering processes remain, in general, not well understood.

[3] *Lynch and Hudnut* [2008] describe a system of mud volcanoes, mound springs, and mud pots in the Imperial Valley, California, which are the focus of this study. The Imperial Valley mud volcanoes, located at the intersection of Davis and Schrimpf roads near Niland, California, are particularly interesting in that they lie on the southeastern extension of the San Andreas Fault (Figure 1) and thus their behavior might provide some insight into fault zone permeability. The response of the small, natural, Imperial Valley mud volcanoes to earthquakes may also provide some insight into the response of larger mud volcanoes that have responded to earthquakes in the past [e.g., *Chigira and Tanaka*, 1997; *Mellors et al.*, 2007; *Bonini*, 2009a; *Manga and Brodsky*, 2006].

[4] We carried out field work in the Imperial Valley on 13 March 2010, 21 March 2010, 6 April 2010, and 12 May 2010. The timing of the 4 April 2010 M_W 7.2 El Mayor-Cucapah event was serendipitous in that we were able to make measurements in a short period of time both before and after the event. During each field campaign, we measured temperature in mud volcanoes and surrounding springs and gas seeps, measured gas discharge where possible, documented the presence of fresh eruptive deposits, and sampled mud for rheological measurements. Our field observations indicate that there was a postseismic increase in gas discharge and eruptive activity at the mud volcanoes. Theory, laboratory measurements of mud rheology, and field observations indicate that transient permeability enhancement is the most plausible mechanism to explain the changes in eruptive activity.

2. Background

2.1. Davis-Schrimpf Mud Volcanoes

[5] *Kopf* [2002] defines a mud volcano as a surface expression of mud that originated at depth. The Davis-Schrimpf mud volcanoes are pictured in Figure 2. The small stature of the mud volcanoes in the Imperial Valley (less then 5 m) categorizes them as "mud lumps" [*Kopf*, 2002] and *Svensen et al.* [2009] have labeled them "hydrothermal seeps," in part because there is very little net exhumation of mud from the subsurface. We will nevertheless continue to refer to these constructional, steep-flanked features as mud volcanoes, and note that *Bonini* [2009b] used the same

[1]Department of Earth and Planetary Science, University of California, Berkeley, California, USA.

0148-0227/10/2010JB007737

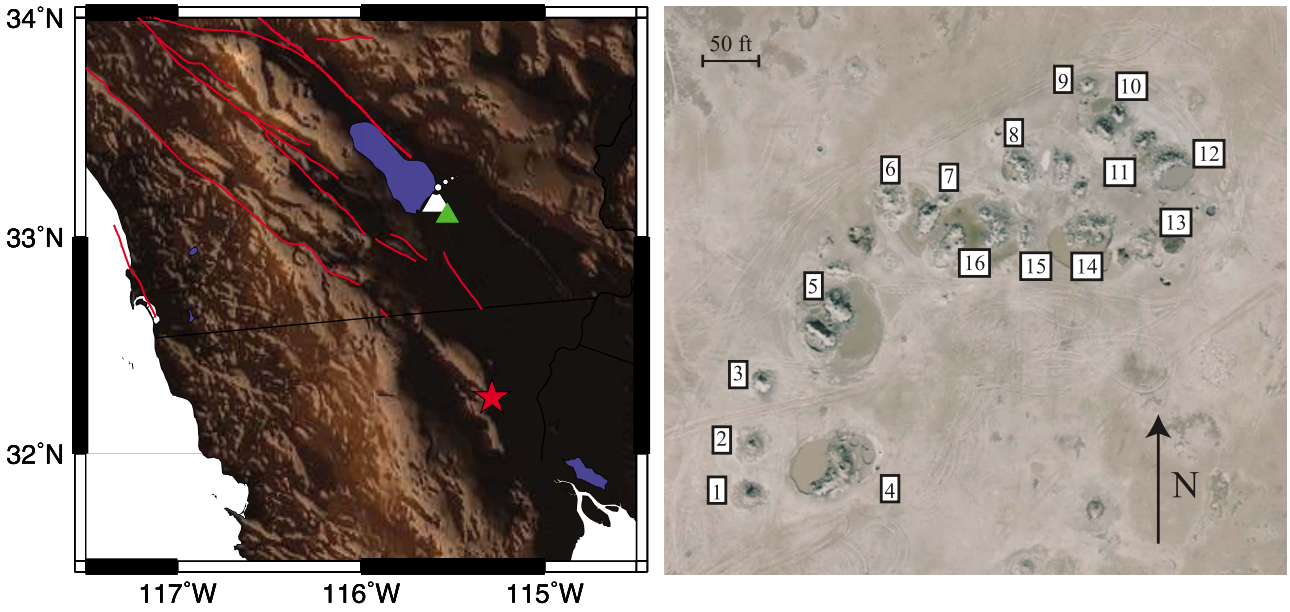

Figure 1. (left) Map of study location, showing major faults in red. Red star indicates epicenter of El Mayor-Cucapah event. Green triangle indicates location of Wildlife Liquefaction Array (WLA). White triangle indicates location of mud volcanoes, seen in (right) an aerial photograph at intersection of Davis and Schrimpf roads near Niland, California.

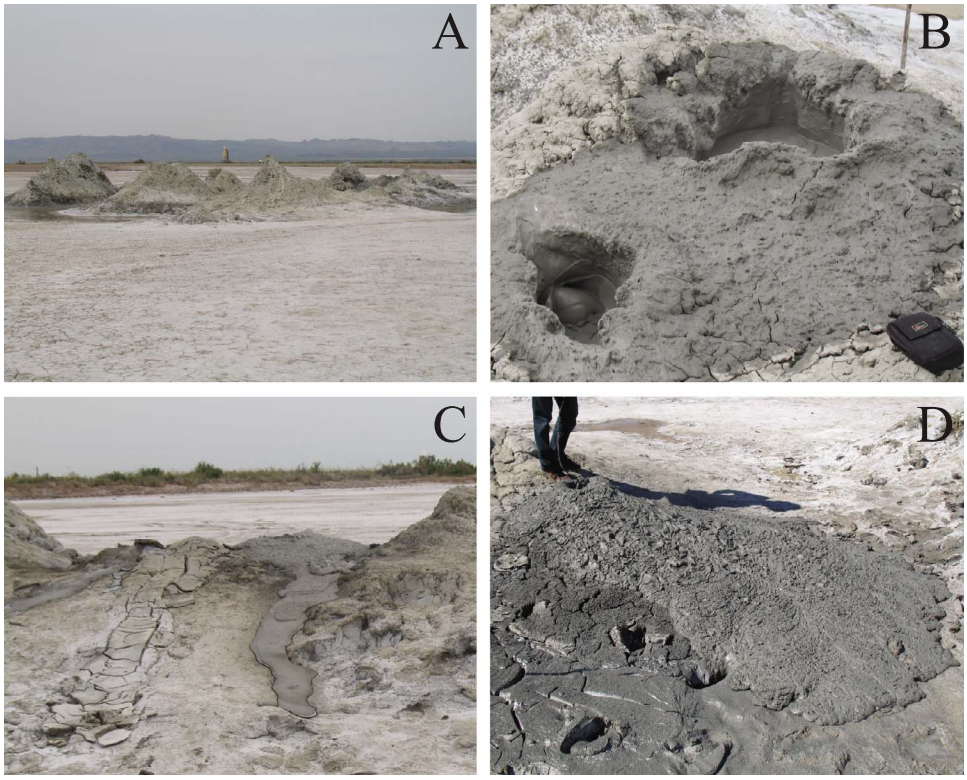

Figure 2. (a) Field of mud volcanoes at the Davis-Schrimpf location. (b) Some of the mud volcanoes have craters filled with bubbling mud, as seen in this picture. (c) The dry mudflow on the left was active on 13 March 2010 but completely dry by 20 March 2010, the date of this photo. The flow to the right was active at the time of the photograph. (d) Very large, fresh flow seen on 6 April 2010. Thermistor probe is in the vent at upper left, where we measured a gas flux of 22 LPM.

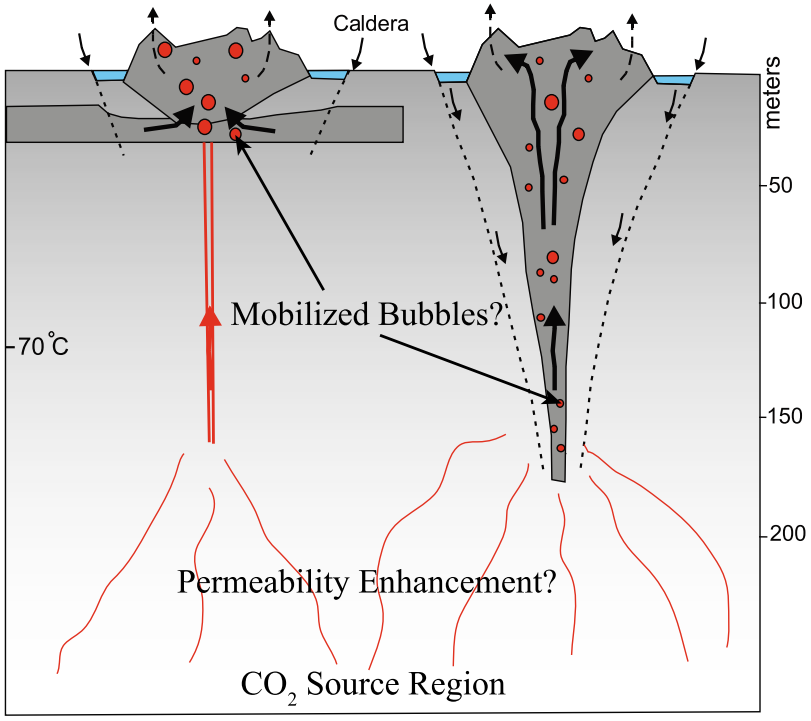

Figure 3. Schematic of two possible mud volcano plumbing systems, modified from *Svensen et al.* [2009]. CO_2 (red bubbles and pathways) is produced at depth in the Salton Sea Geothermal System (SSGS) and travels upward through a porous reservoir. The uppermost 200 m of the system consist of Colorado River deltaic and lacustrine deposits, the source of the erupting mud. The dark arrows indicate the path traveled by mud as it is recycled during mud volcano construction and collapse. Of the two scenarios depicted, *Svensen et al.* [2009] favored the model on the right.

terminology to describe morphologically similar features in the northern Apennines.

[6] The Davis-Schrimpf mud volcanoes considered here are surface expressions of the Salton Sea Geothermal System (SSGS), an area of active geothermal power production [*Bertani*, 2005] and past commercial CO_2 extraction [*Muffler and White*, 1969]. The near-surface geotherm in the SSGS is exceptionally steep. *Helgeson* [1968] reported temperatures as high as 300°C at 3000 ft (914 m), and heat flow in the area can reach 1200 mW m^{-2} [*Elders and Sass*, 1988]. The temperature profile through the SSGS reservoir is isothermal, owing to convection. *Williams and McKibben* [1989] suggest that the intersection between near-surface conductive and deeper convective geotherms results from a stably stratified brine interface rather than a lithologic (permeability) contrast, the interpretation favored by previous authors [e.g., *Helgeson*, 1968; *Younker et al.*, 1982; *Randall*, 1974]. The SSGS is contained within a 6000 m thick sequence of sedimentary rocks, the uppermost ~200 m of which is composed of unconsolidated lacustrine and Colorado River deltaic sediments [*Younker et al.*, 1982]. These sediments are underlain by evaporite deposits. The near-surface strata appear to be the source of the erupting mud, whereas the CO_2 is believed to come from greater depths [*Robinson et al.*, 1976; *Svensen et al.*, 2007], where it is produced through metamorphic decarbonation reactions at temperatures of at least 125°C [*Muffler and White*, 1969]. The details of the subsurface gas and mud plumbing system are not fully understood, but two possible configurations based on *Svensen et al.* [2009] are depicted in Figure 3. Regardless of its depth of production, CO_2 is present at shallower depths; *Kelley and Soske* [1936] note that CO_2 extraction wells were drilled in the late 1920s to a producing horizon between 400 and 500 ft (123 and 152 m) where pressures were between 200 and 300 psi (1.4–2.1 MPa), somewhat in excess of hydrostatic pressure at these depths.

[7] *Sturz et al.* [1992] visited the Davis-Schrimpf mud volcanoes in 1985, 1991, and 1992 and measured mud temperatures between 18 and 32°C and mud composition (45–70% smectite, 20–35% illite, 10–20% kaolinite). *Svensen et al.* [2009] deployed temperature probes in two of the Davis-Schrimpf mud volcanoes and two pools adjacent to the volcanoes between 18 December 2006 and 19 March 2007. This deployment helped establish the recent natural temperature variability inside the mud volcanoes and demonstrated that there is no correlation between temperature changes and tidal forcing. The minimum temperature recorded by *Svensen et al.* [2009] was 37.3°C, the highest recorded temperature was 69.7°C, and the standard deviations were 4.0 and 6.4°C for the two features instrumented. There were no earthquakes of sufficient size during the deployment of *Svensen et al.* [2009] to produce changes in temperature at the mud volcanoes. Although the temperatures measured by *Sturz et al.* [1992] are remarkably lower than those measured by *Svensen et al.* [2009], we cannot speculate as to whether there was a general trend in the mud volcanoes' temperature between 1992 and 2006.

2.2. Response to Earthquakes

[8] Like other hydrologic features, mud volcanoes sometimes respond to earthquakes. *Mellors et al.* [2007] found that large mud volcano eruptions in Azerbaijan occur in the two days following a major earthquake more often than would be expected by chance. *Bonini* [2009a] identified several earthquake-eruption pairs among documented eruptions of Sicilian mud volcanoes. Mud volcanoes (*solfataras*) very similar in appearance to the Davis-Schrimpf mud volcanoes near Volcano Lake, Mexico and associated with the Cerro Prieto geothermal field [*Randall*, 1974] responded to the 1915 Imperial Valley earthquake [*Beal*, 1915] and to the 29 November 1852 Fort Yuma event [*Townley and Allen*, 1939]. The response of these mud volcanoes to shaking was accompanied by other dramatic hydrologic responses. The 1852 Fort Yuma event triggered the eruption of a geyser near Volcano Lake whose plume reportedly reached an elevation of 800–1000 ft (244–205 m) [*Balderman et al.*, 1978].

2.3. El Mayor-Cucapah Earthquake

[9] The 4 April 2010 El Mayor-Cucapah earthquake occurred on the Laguna Salada fault system in northern Mexico. Rupture propagated unilaterally northeastward to a terminus near the Mexico-California border, producing enhanced shaking in the Salton Trough [*Hudnut et al.*, 2010]. The event accommodated both east-down and right-lateral slip along the Pacific-North American plate boundary. The earthquake was accompanied by extensive surface rupture and liquefaction was widespread in the near field [*King et al.*, 2010; *Pridmore et al.*, 2010]. Well-level responses were common throughout the western United States (Figure 4).

3. Methods

[10] We measured temperature at each of the mud volcanoes using a thermistor and gas discharge using a funnel (22 cm diameter) connected to Cole-Parer gas flow meters. The stated accuracy of the flow meters is ±5% and repeatability is ±0.5%. We used the same equipment and employed the same division of labor (placing funnel, taking measurements) on each field trip. Our best estimate of the human error associated with reading the gas flow meters is ±0.5 LPM for measured fluxes less than or equal to 10 LPM and ±5 LPM for fluxes greater than 10 LPM.

[11] We used a Haake Rheoscope-1 cone-plate rheometer to characterize the material properties of mud collected from the vents of four of the Davis-Schrimpf mud volcanoes. The cone has a diameter of 60 mm with a bevel angle of 4° and a minimum gap thickness of 139 μm, larger than the particle size of the mud (Figure 5). The mud was stored in two layers of gas-impermeable plastic bag between sample collection and analysis to minimize desiccation and refrigerated to retard any chemical reactions. We measured the response of mud under steady shear and oscillatory shear. In the steady shear experiments, we loaded the mud samples, measured yield strength and measured the applied stress as a function of strain rate. We measured yield strength using a method suggested by *Dubash and Frigaard* [2007], whereby constant stress was applied for 120 s and the total strain at the end of this period was recorded. In the oscillatory shear experiments, we loaded the samples, presheared them for 10 s at a strain rate of 1 s^{-1}, and then deformed them under oscillatory shear at fixed frequencies of 0.2, 1.0, and 10 Hz while controlling strain amplitude between 10^{-4} and 10^{-2}. These strain amplitudes and frequencies are comparable to those imposed by earthquakes, discussed later and shown in Figure 6. For each data point in the oscillatory shear experiments, the sample was presheared for three cycles and then measurements were averaged over five cycles. The oscillatory strain experiments allow us to measure the storage and loss moduli of the mud, assuming that it behaves as a Maxwell viscoelastic material. We also retained the raw data for stress and strain as a function of time, which allowed us to confirm that the Maxwell model was appropriate. The equipment and methodology used here is identical to that used by *Sumita and Manga* [2008] and was also used to characterize mud erupted from the Sidoarjo mudflow in Indonesia [*Manga et al.*, 2009].

[12] We obtained waveforms for the El Mayor-Cucapah event at the Wildlife Liquefaction Array (WLA, location indicated by green triangle in Figure 1), which, at 12.3 km, is the closest strong motion seismometer to the Davis-Schrimpf location. Waveforms (Figure 6) were obtained from IRIS for two accelerometers at the WLA site: a borehole instrument at a depth of 100 m and a surface instrument. We removed the mean from, detrended, and then integrated the seismograms to obtain displacement time series. We applied a high-pass filter with a pass band above 0.02 Hz to remove spurious long-period signals. Shear strain can be approximated from peak ground velocity using the empirical relationship $\gamma \sim (\mathrm{PGV})/V_S$ or from peak ground acceleration using $\gamma \sim 1.2z(\mathrm{PGA})/V_S^2$ [*Wang et al.*, 2003]. Assuming $V_S = 500$ m s^{-1} (typical of unconsolidated sediments), both of these scaling relations yield estimates for γ on the order of 1%. We also computed displacement gradients ($\partial u_{Radial}/\partial z$ and $\partial u_{Tangential}/\partial z$) directly using the surface and 100 m depth records and found a peak shear strain of 1.2% (Figure 6), in good agreement with the scaling relationships. Displacement gradients computed with this method place a lower bound on the true displacement gradient.

[13] We used Coulomb version 3.1.09 [*Lin and Stein*, 2004; *Toda et al.*, 2005] to calculate volumetric strain associated with the earthquake using the moment tensor solution from the Global CMT Project's catalog (globalcmt.org) [*Dziewonski et al.*, 1981] and fault geometry from the empirical scaling of *Wells and Coppersmith* [1994].

[14] The United States Geological Survey (USGS) maintains monitoring stations for ground water table in several locations, mostly near major cities, in the western United States. We compiled all of the well water level data for Arizona, California, Colorado, Idaho, Montana, Nevada, Oregon, Utah, and Washington and searched manually for a response coincident in time with the El Mayor-Cucapah event. Of the 154 records obtained, 63 showed a response (well locations and responses shown in Figure 4). Most of the wells have a sampling interval of 15 min except for several that record only twice per hour. The most distant well that showed a response was 1749 km from the epicenter.

4. Results

4.1. Field Measurements

[15] We measured gas flow at 5 features on 13 March 2010, 8 features on 20 March 2010, 18 locations on 6 April 2010, and 12 locations on 12 May 2010. The average flow

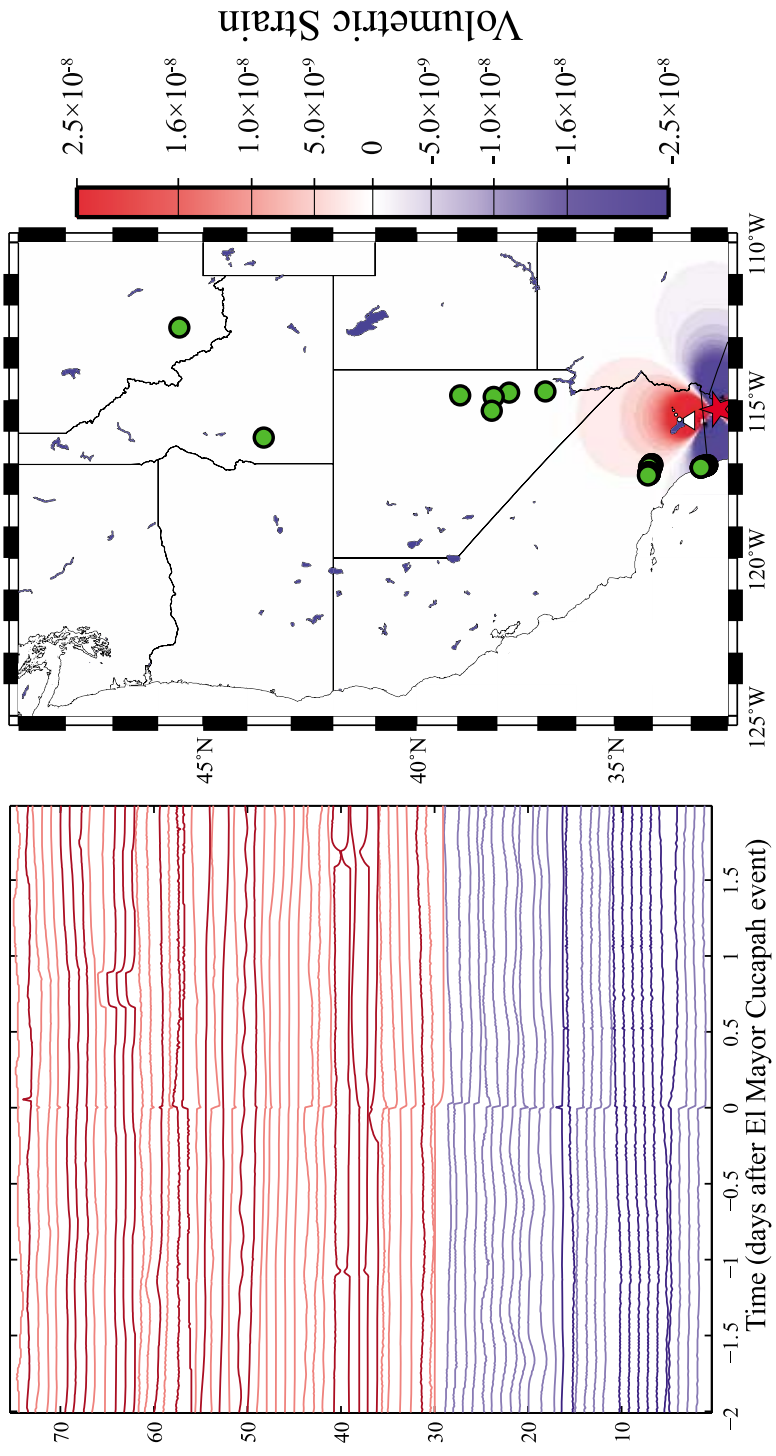

Figure 4. (right) Map indicating location of wells in the western United States (green circles) that responded to the El Mayor-Cucapah earthquake (red star marks epicenter). Background field is dilatation: red and blue represent expansion and contraction, respectively. (left) Water level records (distance below surface) in wells that showed a response. Each well's record has been normalized with respect to its maximum absolute value in the time interval plotted. Zero time corresponds to time of El Mayor-Cucapah event. Water level records are sorted bottom to top in order of increasing epicentral distance, and color indicates whether the well experienced contraction (blue) or expansion (red). Darker colors indicate a record that showed a decrease in water level (increase in distance below surface), and lighter colors indicate an increase in water level. There does not appear to be a correlation between the sign of the volumetric strain and the sign of the change in water level.

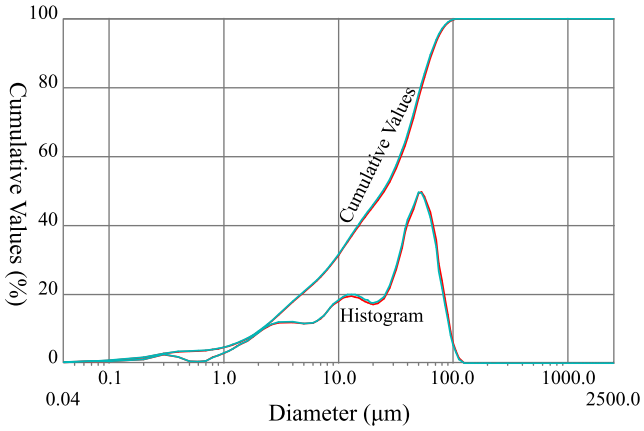

Figure 5. Measured particle size in mud from Davis-Schrimpf mud volcano 12. Blue and red curves show two measurement runs of the same sample. Particle diameters representing the 10th, 50th, and 90th percentiles of the cumulative particle size distribution are D_{10} = 2.13 μm, D_{50} = 24.31μm, and D_{90} = 63.81 μm.

per measurement was 7.0 liters per minute (LPM), 7.6 LPM, 12.5 LPM, and 9.5 LPM, respectively, with standard deviations of 2 LPM, 1.35 LPM, 5.3 LPM, and 3.3 LPM, respectively. Figure 7 is a compilation of our gas flux measurements (tabulated in the auxiliary material), showing increased gas flux on 6 April 2010.[1] The increase in gas flux is the most robust evidence for a postseismic response at the mud volcanoes. The pathways through which gas escapes appear to be stable over the time period of our study, although this is clearly not the case over year-to-decadal time scales [*Sturz et al.*, 1992]. Estimating the total change in gas flux following the earthquake is difficult because some gas discharge locations became dangerous or otherwise inaccessible due to the changing depth of pools and reconfiguration of crater rim material. Therefore, we believe that the change in average discharge per measurement site is the best proxy for increased gas flux.

[16] We measured temperature at 14 mud volcano vents on 13 March 2010, 7 on 20 March 2010, 16 on 6 April 2010, and 12 on 12 May 2010. The average temperatures were 44.0°, 56°, 46.6°, and 56.9°with standard deviations of 11.0°, 5.6°, 11.8°, and 8.6°. Figure 7 is a compilation of all of the temperature measurements, which are also available in the auxiliary material. There is no discernible postseismic temperature response and all of the values measured are within 3° of the range documented by *Svensen et al.* [2009] and *Sturz et al.* [1992].

[17] In addition to the quantitative measures of gas flux and temperature, we also noted the number of fresh flow features. We can roughly constrain the age of surface flows based on appearance; Flows that were active on 13 March 2010 and inactive on 20 March 2010 no longer had moist surfaces. We observed four fresh flows on 13 March 2010, four on 20 March 2010, eight on 6 April 2010, and five on 12 May 2010. The flows observed on 6 April 2010 included one that had erupted from a new vent, at which we also measured a gas flux of 22 LPM, more than twice the largest

[1] Auxiliary materials are available in the HTML. doi:10.1029/2010JB007737.

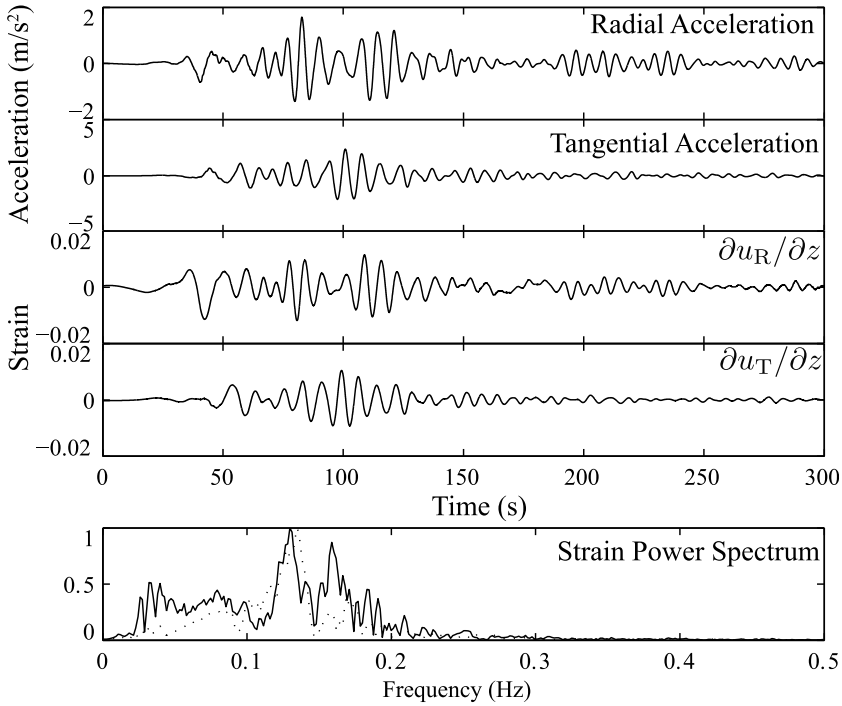

Figure 6. Waveforms from Wildlife Liquefaction Array (green triangle in Figure 1), 100 m depth, for El Mayor-Cucapah event. Shear strain in the uppermost 100 m reached a maximum value of 1.2%. Two strain power spectra are plotted: radial (solid line) and transverse (dashed line).

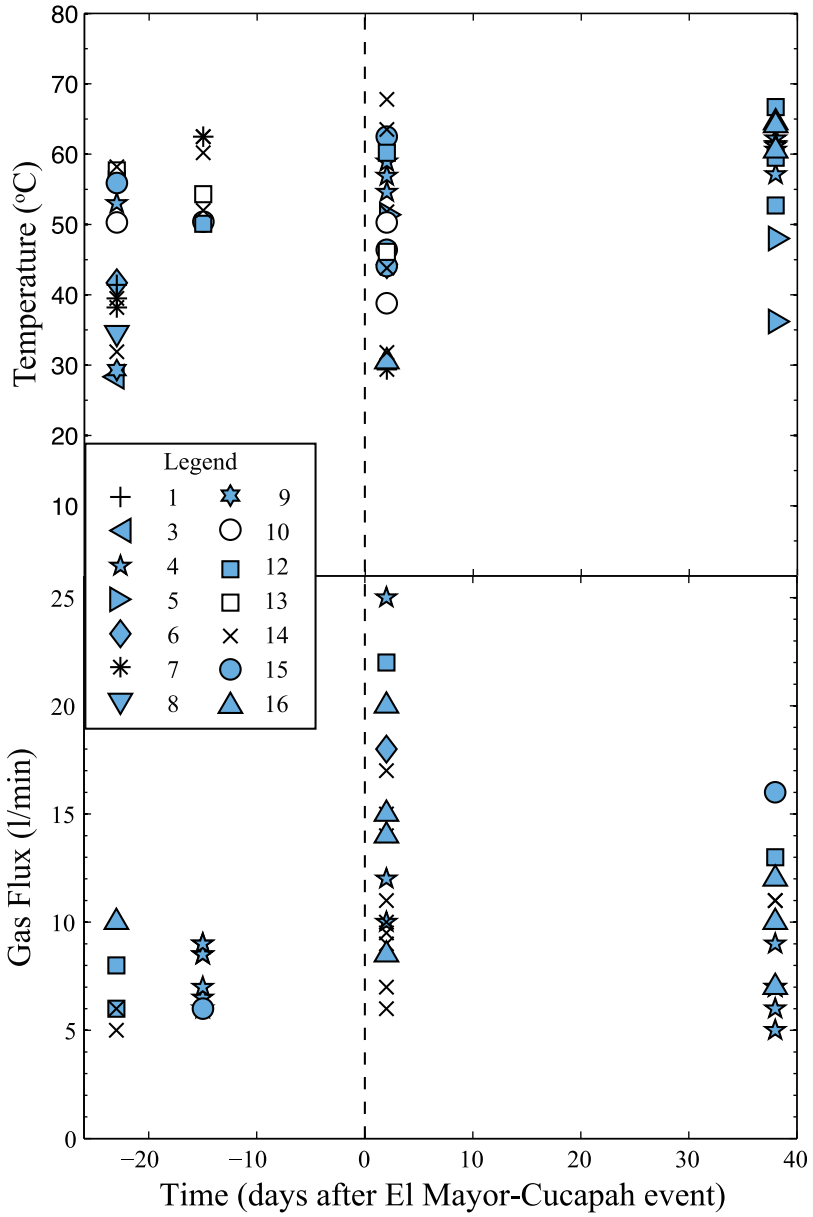

Figure 7. Compilation of (top) temperature and (bottom) gas flux measurements made at Davis-Schrimpf mud volcanoes as a function of time. Symbols correspond to individual mud volcanoes as numbered in Figure 1. The vertical dashed line indicates the time at which the El Mayor-Cucapah event occurred. Repeated glyphs on a given day indicate that there were multiple active vents on the mud volcano, and each glyph corresponds to a measurement made at one of the vents. The mean gas flux increased by about 70%, and the maximum gas flux was 150% larger than any pre-earthquake value. We cannot discern any seismic response in the temperature data.

pre-earthquake value at any vent. This vent was extinct on 12 May 2010, with no measurable or audible gas flux.

4.2. Laboratory Measurements

[18] We had the grain size distribution in five of our samples measured using a CILAS 1190LD trilaser particle size analyzer. We chose three samples from the same crater of mud volcano 12 (Figure 1), collected on 13 March 2010, 20 March 2010, and 6 April 2010 and two atypical samples, one from a very low viscosity pool on 6 April 2010 and a second from the interior of a large, fresh mud flow on 6 April 2010. The samples were placed in an ultrasonicator for 60 s prior to measurement and were ultrasonicated continuously during measurement to minimize agglomeration. The grain size distribution, shown in Figure 5, was very consistent among the mud volcanoes. The average 50th percentile particle diameter is 24.31 μm and the peak of the grain size distribution is consistently about 50 μm among all of the samples. We measured the water content of each of the samples for which we analyzed grain size. The large, fresh

mudflow had the lowest water content, 33% by mass, the low-viscosity pool had the highest, 48%, and the mud in the craters was on average 40% water with a standard deviation of 1% among six samples.

[19] Our analyses of the erupted muds from the Davis-Schrimpf mud volcanoes indicate that the mud has a yield strength of 52 Pa at 40 wt% H_2O and 294 Pa at 33 wt% H_2O and is shear thinning (Figure 8a). The unidirectional shear experiments produced measurements of effective viscosity that are well approximated by the empirical relationship

$$\mu = 10^{1.8}\dot{\epsilon}^{-0.82}(40\ \text{wt\% } H_2O)$$
$$\mu = 10^{2.3}\dot{\epsilon}^{-0.83}(33\ \text{wt\% } H_2O) \quad (1)$$

where μ has units of Pa s and $\dot{\epsilon}$ has units s^{-1}. Figure 8b shows the viscosity measurements for both samples. Under oscillatory shear, the mud experiences a reduction of strength at shear strains between 10^{-3} and 10^{-2} irrespective of frequency (Figure 8c), similar to mud from the Sidoarjo mudflow [*Manga et al.*, 2009].

[20] We used X-ray diffraction to measure the composition of two mud samples. We identified the minerals kaolinite, muscovite, montmorillonite, dolomite, calcite, and albite in both of the mud samples. One of the samples contained orthoclase. We were unable to measure the relative abundances of the various minerals present using this technique.

5. Discussion

[21] The epicenter of the El Mayor-Cucapah earthquake was 96.6 km from the mud volcano location. Figure 9 shows that this earthquake was close enough that a mud volcano response is not unexpected based on empirical magnitude-distance-triggering relationships developed for mud volcanoes and other hydrologic features [*Wang and Manga*, 2010]. Our field observations show that the mud volcanoes did respond to the El Mayor-Cucapah earthquake. To demonstrate statistically that a response occurred, we divide the gas flux measurements into two groups: (1) data from 6 April 2010 and (2) all other data. We wish to ascertain whether the mean or median of group 1 is significantly different from group 2. We used the Shapiro-Wilk test of normality [*Shapiro et al.*, 1968] and found that we could reject the null hypothesis that the data is normally distributed. Because both data sets are not normally distributed, we chose to use the Mann-Whitney U test [*Hollander and Wolfe*, 1999, p. 125], the result of which allows us to reject the null hypothesis that the two groups are independent samples of identical distributions with equal medians at the $\alpha = 0.01$

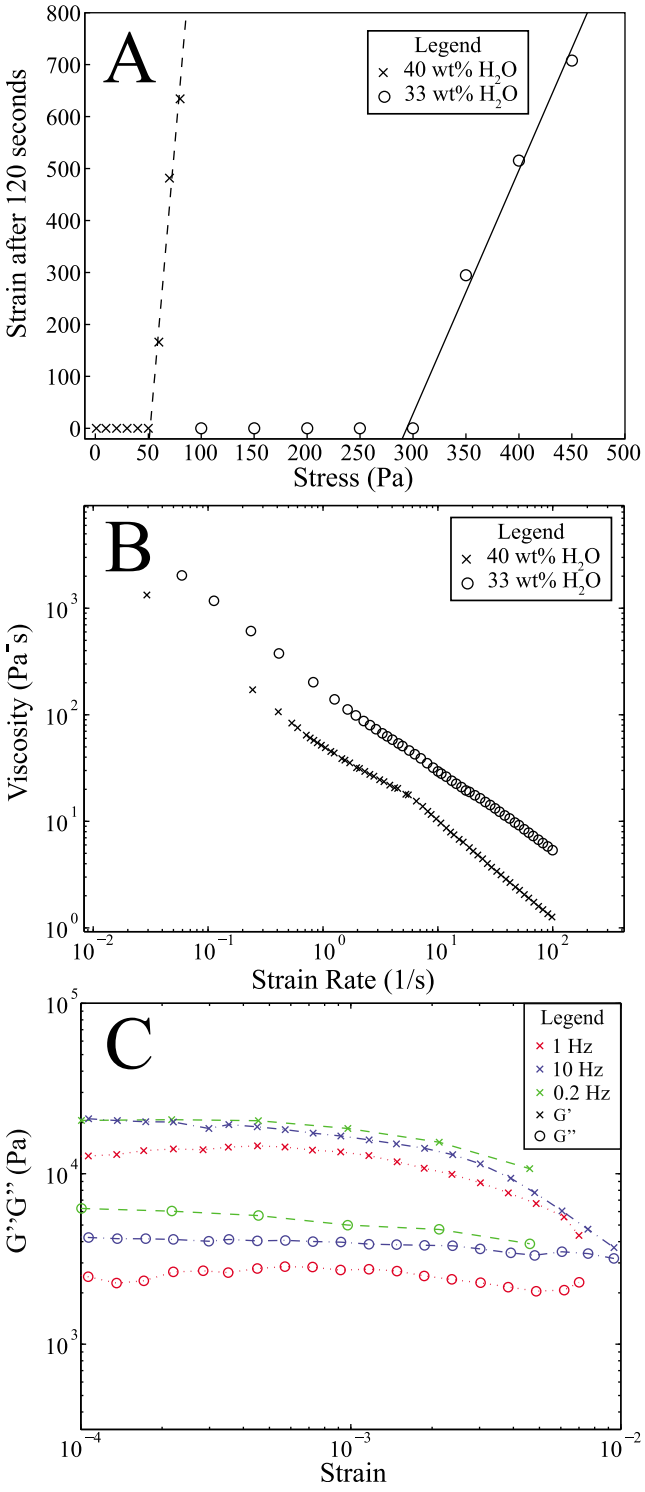

Figure 8. (a) Yielding behavior of mud from crater of Davis-Schrimpf mud volcano 12 (cross) and from the interior of a viscous mudflow sampled on 6 April 2010 (circles). The dashed and solid lines are fits to last three data points (crosses) and last four data points (circles), respectively. The best fit lines intersect the horizontal axis at 52 Pa (crosses) and 294 Pa (circles), estimates of the yield strength of the muds. (b) Effective viscosity of the same mud samples used in Figure 8a, which depends onstrain rate. Note that the mud with higher water content (crosses) is 3–4 times less viscous than the mud with lower water content (circles). (c) Storage modulus (G', crosses) and loss modulus (G", circles) of mud (low-viscosity sample from Figures 8a and 8b) as a function of frequency and strain amplitude under oscillatory shear. The strain frequencies and amplitudes used here are representative of those experienced at the WLA site during the El Mayor-Cucapah event. We interpret the decrease in G' between strain amplitudes of 10^{-3} and 10^{-2} as representing the onset of fluid-like behavior.

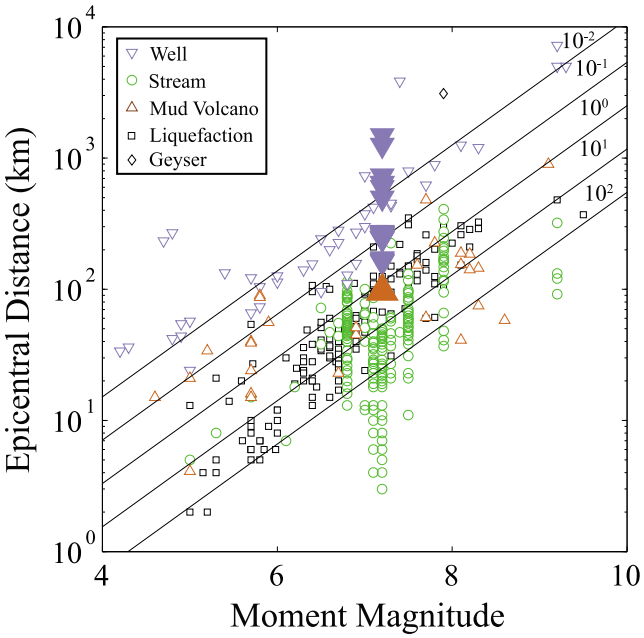

Figure 9. Documented occurrences of liquefaction, stream flow changes, mud volcano eruptions, and well water-level changes in response to earthquakes as a function of distance from epicenter and moment magnitude as compiled by *Wang and Manga* [2010]. Large filled symbols correspond to well (blue) and mud volcano (brown) responses to the El Mayor-Cucapah event. Diagonal lines are contours of constant seismic energy density in J m^{-3} [*Wang and Manga*, 2010], which we expect to define the region in which triggering is possible. The Davis-Schrimpf mud volcanoes are within the range of parameter space where triggering of mud volcanoes has been previously documented.

significance level. We now turn our attention to the mechanism responsible for this response.

[22] *Manga et al.* [2009] reviewed possible triggering mechanisms: (1) volumetric changes due to static stress transfer [*Walter and Amelung*, 2007], (2) dilatancy [*Wang et al.*, 2001], (3) liquefaction [*Wang*, 2007], (4) destabilization of gas hydrates [*Obzhirov et al.*, 2004; *Mau et al.*, 2007], (5) mobilization of preexisting bubbles [*Steinberg et al.*, 1989; *Sahagian and Proussevitch*, 1992], (6) increasing permeability or opening fractures [*Rojstaczer et al.*, 1995; *Elkhoury et al.*, 2006; *Wang et al.*, 2004a, 2004b; *Brodsky et al.*, 2003], and (7) enhanced gas production. We consider mechanism 1 unlikely because the Davis-Schrimpf mud volcanoes experienced volumetric expansion in the El Mayor-Cucapah event (Figure 4), which we do not expect to expel pore fluids, but could enhance permeability, in which case we would treat this mechanism concurrently with mechanism 6. Furthermore, we disfavor this mechanism because the amplitude of static volumetric strain (10^{-8}) is much smaller than the amplitude of dynamic shear strain (10^{-2}) at the Davis-Schrimpf site. Mechanism 2 is not applicable in this case because the Davis-Schrimpf location is not in the near field of the El Mayor-Cucapah event. Mechanism 3 is unlikely to have occurred because liquefaction was not observed at the Wildlife Liquefaction Array [*Pridmore et al.*, 2010]. Mechanism 4 may be immediately removed from further consideration because gas hydrates are not stable in this geologic setting.

[23] Like their magmatic cousins, mud volcanoes are driven by gas escape. Therefore it is natural to consider triggering mechanisms involving gas bubbles such as nucleation [*Steinberg et al.*, 1982], bubble growth [*Hsieh*, 1961; *Sturtevant et al.*, 1996], and mobilization [*Sahagian and Proussevitch*, 1992]. Gas bubbles trapped in a yield strength fluid may be mobilized if seismic shaking temporarily weakens the material. This mechanism was considered for earthquake triggering of the Sidoarjo mudflow but rejected due to very low strain amplitudes [*Manga et al.*, 2009]. However, the El Mayor-Cucapah event produced dynamic strains larger than 1% in the Imperial Valley, large enough to weaken mud (Figure 8).

[24] In general, a bubble may rise through a yield strength fluid only if the buoyancy force resulting from its density is sufficiently large to overcome the yield strength (τ_y). The measured yield strength of mud from the mud volcano craters is 52 Pa and the yield strength of mud from the low water content flow is 294 Pa. Because the mud is able to erupt and form flows of finite thickness, we expect the yield strength to limit flow thickness ($h \sim \tau_y/(\rho g) \sim 2.5$ mm – 1.5 cm). The measured yield strengths are qualitatively consistent with the thickness of flows that we observed in the field.

[25] *Dubash and Frigaard* [2004] studied the conditions necessary to arrest bubbles in a Herschel-Bulkley (non-Newtonian, yield stress) fluid. The Herschel-Bulkley rheological model was chosen specifically for application to bubbles in drilling muds. For permanently immobilized, spherical bubbles, *Dubash and Frigaard* [2004] give the condition $\tau_y < \Delta\rho g R$ where $\Delta\rho \sim 2000$ kg m^{-3} is the density difference between the bubble and fluid, g is gravitational acceleration, and R is a characteristic length scale for the bubble. We define a critical bubble as the largest bubble whose buoyancy is unable to overcome the mud's yield strength, and consider the possibility that a coseismic, transient reduction in yield strength mobilized critical bubbles. The critical bubble radius R_C is between ~2.5 mm (using the lowest measured yield strength) and 1.5 cm (assuming the highest measured yield strength). The radius of bubbles bursting in the mud volcano craters is about 10 cm. Assuming that a critical bubble conserves mass during ascent, the depth at which the critical bubble becomes mobilized can be calculated. We assume that $V_{surf}/V_0 = P_0/P_{surf}$ where the subscript 0 refers to the depth of mobilization, yielding 4×10^6 Pa $< P_0 < 8 \times 10^8$ Pa, corresponding to depths between 200 m and 40 km if $\rho = 2000$ kg m^{-3}, implying expansion from a source region below the deltaic and lacustrine deposits. Because the mud source is believed to be in the deltaic and lacustrine deposits, we interpret the large depth of mobilization as evidence that bubble coalescence occurs during ascent.

[26] In order to quantify the time scale associated with a mud volcano response due to mobilization of bubbles, we must estimate bubble rise velocity. Mud is non-Newtonian and has a yield strength, but we can place an *upper bound* on the true bubble rise velocity by approximating mud as a Newtonian fluid. Bubble ascent velocity is limited not only by rheology but also by the finite width of the conduits

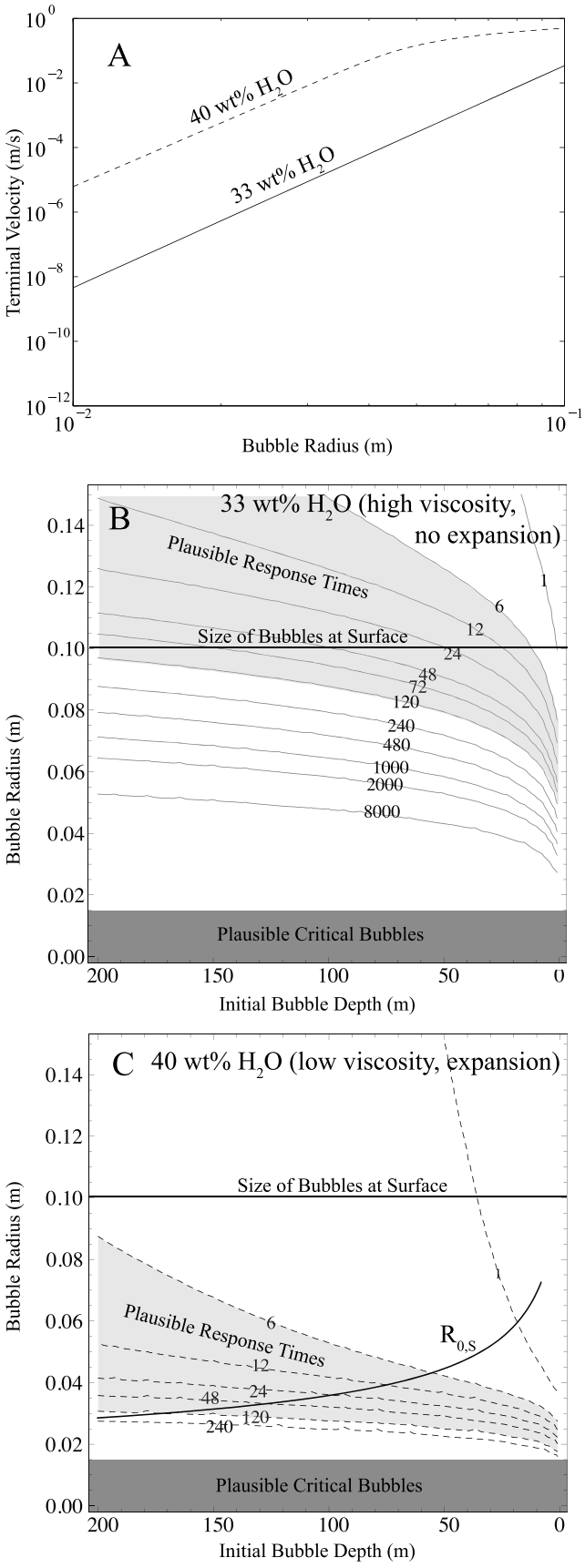

through which bubbles rise. Bubble ascent rate through an unbounded Newtonian fluid is given by $U = R^2\Delta\rho g/(3\mu)$ in the creeping (Stokes) flow regime. At Reynolds number (Re) > 0.1 it is necessary to adopt a parameterization that accounts for inertia. We use the parameterization given by *Clift et al.* [1978, p. 206] for terminal velocity of millimeter- to decimeter-sized bubbles in a Newtonian fluid:

$$2\mathrm{Re}^2 + 6\mathrm{Re}[(2+3\kappa)/(1+\kappa)] - \mathrm{Ar} = 0 \qquad (2)$$

where $\kappa = \mu_{gas}/\mu_{liquid}$ is a viscosity ratio, $\mathrm{Ar} = g\rho_{liquid}\Delta\rho R^3/\mu^2$ is an Archimedes number, and R is bubble radius. We use the best fit to our viscosity measurements (Figure 8), given by equation (1).

[27] We approximate strain rate as $\dot{\epsilon} = U/R$, and assume that $\mu_{\mathrm{gas}} = 1.5 \times 10^{-5}$ Pa s and $\rho_{liquid} = 2000$ kg m^{-3}. We solved equation (2) numerically for various choices of R and both parameterizations of μ. Figure 10 shows that ascent velocities are vanishingly small (10^{-5} – 10^{-8} m s^{-1}) for 1 cm bubbles but become large (0.1 – 1 m s^{-1}) for decimeter-sized bubbles.

[28] The time scale associated with the bubble mobilization response mechanism is strongly dependent on the choice of bubble size and assumed depth of bubbles prior to the onset of shaking, but in general can be constrained using the maximum radius of bubbles bursting at the surface (0.1 m) and the thickness of the deltaic and lacustrine deposits (200 m). We calculated bubble ascent times as a function of initial bubble size and initial bubble depth using both viscosity parameterizations and using (1) constant bubble radius and (2) allowing bubble radius to change with pressure (depth) according to $V/V_0 = P_0/P$. For a given initial radius and depth, bubbles ascend most quickly when they expand and viscosity is low (Figure 10c) and most slowly when they do not expand and viscosity is high (Figure 10b). We use these two bounding scenarios to test the plausibility of the bubble mobilization mechanism. In Figures 10b and 10c, we have shaded in light grey the region corresponding

Figure 10. (a) Terminal velocity of bubbles in a Newtonian fluid, from numerical solution of equation (2), using measured mud viscosity (shown in Figure 8b). Bubbles of decimeter size (comparable to those observed bursting in mud volcanoes) rise at 0.03–0.50 m s^{-1}. Bubbles smaller than a few centimeters are essentially immobile. The calculated velocity is an upper bound on the rise speed through mud. (b and c) Contour plots of bubble ascent time (hours) for different choices of initial bubble depth and bubble radius. Figure 10b assumes the most viscous, and Figure 10c the least viscous, measured rheology. In Figure 10b we assume that bubble size remains constant during ascent, and in Figure 10c we assume that bubbles conserve mass and expand in response to changing pressure. Figures 10b and 10c should be interpreted as upper and lower bounds, respectively, on the response time. The dark shaded region at the bottom of Figures 10b and 10c denotes the plausible size range of critical bubbles (defined in text), and its lack of overlap with the light shaded region disfavors the bubble mobilization response mechanism. The curve marked $R_{0,S}$ indicates the size of bubble at depth that expands to a radius of 0.1 m at the surface.

to ascent times of 6 h to 5 days, representing plausible response time scales and we have shaded dark grey the region corresponding to plausible critical bubble sizes. The lack of overlap between light and dark shaded regions indicates that the mobilization of critical bubbles cannot produce an increase in gas flux over the observed response time scale.

[29] If critical bubbles become mobilized and subsequently coalesce, they will ascend more rapidly than the original critical bubbles. In Figure 10c, the dark line marked $R_{0,S}$ indicates the initial radius of bubbles that expand to have a radius of 0.1 m at the surface. This curve passes through the light grey region of plausible response times, which indicates that if coalescence happens quickly, the bubble mobilization mechanism may be viable. The rate of coalescence of centimeter-sized buoyancy-driven bubbles in the Stokes flow regime was studied by *Manga and Stone* [1995] by solving population dynamics equations and using a coalescence rate based on laboratory experiments. The rate of coalescence of centimeter-sized bubblescan be greatly enhanced over that of spherical bubbles owing to their interaction-induced deformation [*Manga and Stone*, 1994]. The magnitude of deformation scales with the Bond number $\mathcal{B} = \Delta\rho g R^2/\sigma$, a measure of the relative importance of buoyancy and surface tension forces. Using a surface tension $\sigma = 7 \times 10^{-2}$ Pa m^{-2} and the critical bubble radii previously introduced, we compute $1.8 < \mathcal{B} < 64$. Bubbles smaller than about 4 cm rise at Re < 0.1, so the Stokes flow assumption is valid for critical and near-critical bubbles. The characteristic time scale for bubble interactions is given by $t_c = \mu/(\Delta\rho g r_0 \phi_0)$ where r_0 is initial bubble radiusand ϕ_0 is initial bubble volume fraction. We adopt a range of viscosities of $10^6 - 10^7$ Pa s, characteristic of the viscosities seen by bubbles that are slightly larger than critical. Assuming $\phi_0 = 0.01$ (a guess), we find 2×10^6 s $< t_c < 3 \times 10^6$ s (11.5 days $< t_c <$ 35 days). The rate of coalescence scales linearly with $\mathcal{B}$. However, the mean bubble size does not increase significantly within the first t_c. It thus appears unlikely that coalescence of mobilized bubbles can act quickly enough to produce bubbles sufficiently large to produce the observed response. Furthermore, the bubble coalescence model assumes that the bubbles exist in an unbounded fluid medium. Conduit boundaries limit the interactions between bubbles and hence will tend to retard bubble coalescence, so our estimate of t_c should be interpreted as a lower bound.

[30] In the above calculations, we assumed that the mud in the subsurface, where bubbles might be immobilized, has the same water content as the mud erupted at the surface. There is no reason for this to be true, and the effective viscosity and yield strength of the mud at depth might vary considerably depending on the water content. *Coussot and Piau* [1994] measured the rheology of water-kaolinite mixtures with varying water content and found order-of-magnitude increases in viscosity when solid fraction increased from 15.4% to 27%. We measured a sixfold increase in yield strength when solid mass fraction increased from 60% to 67%. A higher viscosity at depth resulting from lower water content would increase the response time, reducing further the plausibility of the bubble mobilization response mechanism.

[31] The exceptionally slow ascent rate of critical-sized bubbles makes it unlikely that mobilization of critical or near-critical bubbles is the triggering mechanism responsible for the observed change in gas flux. Coseismic strength reduction could also increase the ascent rate of larger than critical bubbles, but the ascent rate would only increase for a short time during and after shaking. We did not observe any hysteresis in the mud samples when we performed oscillatory strain runs in immediate succession. Each of the experimental runs required about 20 min, which, if used as an upper bound on the time scale of strength recovery, cannot explain the observed increase in gas flux two days after the El Mayor-Cucapah event.

[32] Coseismic enhancement of fracture permeability by removal of blockage has been inferred in bedrock aquifers [e.g., *Rojstaczer and Wolf*, 1992; *Rojstaczer et al.*, 1995; *Wang et al.*, 2004b; *Brodsky et al.*, 2003] and laboratory experiments [*Liu and Manga*, 2009; J. Elkhoury et al., Dynamic stress stimulates flow in fractures: Laboratory observations of permeability enhancement, submitted to *Journal of Geophysical Research*, 2010]. The El Mayor-Cucapah event triggered slip on nearby faults including the San Andreas and Superstition Hills faults as well as several faults in the Brawley Seismic Zone [*Treiman et al.*, 2010], and slip may increase fault zone permeability. If the increased gas flux was facilitated by increased fracture permeability, the permeability increase could have occurred in the SSGS reservoir, in the shallow lacustrine and deltaic deposits, or both. The time scale associated with the observed response (less than two days), together with permeability estimates and knowledge of local geology allows us to critically evaluate this mechanism. In the subsequent analysis, we assume that gas bubbles and water comprise the pore fluid in a porous aquifer, whereas when considering the bubble mobilization mechanism we assumed that gas bubbles were a discontinuous phase in a mud continuum. This assumption and the corresponding analysis are reasonable if the mud source is shallow [e.g., *Svensen et al.* 2009] and the permeability enhancement occurs below the mud source depth.

[33] Changes in permeability will result in a redistribution of pore pressure by fluid flow over a characteristic time scale $t \sim d^2/\kappa$ where d is a characteristic depth and κ is a vertically averaged gas diffusivity in the depth interval [0,d]. The strata in the cap rock unit are essentially flat lying, so vertical permeability will be dominated by the least permeable stratigraphic layer, or by fracture permeability. Ongoing gas escape implies that there is significant vertical permeability, which we attribute to fracture permeability. We place a lower bound of 10^{-6} to 10^{-4} m s^{-1} on the hydraulic conductivity using measured hydraulic conductivities in the shallow subsurface of the WLA site [*Youd et al.*, 2004], consistent with intrinsic permeabilities of the types of sediment present. These hydraulic conductivity values are given for water only, but in fact the SSGS is a multiphase system with both liquid and gas present. We assume that in this system, water comprises the continuous phase. In general, the relative permeability of each phase in the system is a function of the volume fractions of each phase, capillary number of the flow, viscosity ratio of the phases, and flow history [*Adler and Brenner*, 1988]. In order to quantify the response time scale, we make use of the hydraulic diffusivity $\kappa = K/S_S$ where K is hydraulic conductivity and S_S is the specific storage. In multiphase systems, each of these parameters is phase-specific. The hydraulic conductivity (K) and permeability (k) are related by $K = k\rho g/\mu$. Noting that k

represents only properties of the porous medium and not the fluid occupying its pores, we estimate the ratio of gas permeability to liquid permeability:

$$K_{gas}/K_{liq} \sim \frac{(10^0 \text{ kg m}^{-3})/(10^{-5} \text{ Pa s})}{(10^3 \text{ kg m}^{-3})/(10^{-3} \text{ Pa s})} = 10^{-1} \quad (3)$$

[34] Specific storage is defined as $S_S = \rho_f g(\alpha + \phi_f \beta)$ where α is the matrix compressibility, β is the fluid compressibility, and ϕ is porosity. Because gases are much more compressible than liquids, we can neglect matrix compressibility and estimate the ratio of $S_{S,\text{gas}}/S_{S,\text{liq}}$ as

$$S_{S,\text{gas}}/S_{S,\text{liq}} \sim \frac{(10^0 \text{ kg m}^{-3}) \times (10^{-5} \text{ Pa}^{-1})}{(10^3 \text{ kg m}^{-3}) \times (10^{-10} \text{ Pa}^{-1})} = 10^2 \quad (4)$$

[35] Therefore, we expect the ratio of diffusivities in identical single phase gas and liquid systems to be $\kappa_{gas}/\kappa_{liq} \sim (K_{gas}/K_{liq})/(S_{S,\text{gas}}/S_{S,\text{liq}}) = 10^{-3}$. This ratio is an upper bound on the diffusivity ratio that we would expect in a system where two phases are present and gas is the dispersed phase, since the relative permeability of the gas phase will be smaller than the permeability in a gas-only system.

[36] If we adopt standard values of 10^0 – 10^3 m^2 s^{-1} for the hydraulic diffusivity of water in unconsolidated sediments [*Roeloffs*, 1996], the corresponding gas diffusivities are 10^{-3} – 10^0 m^2 s^{-1}. The time scale associated with the postseismic gas response could be almost instantaneous or more than a year, assuming a length scale representative of the thickness of the near-surface river and lacustrine deposits, 200 m (Figure 11). Because gas fluxes were significantly higher on 6 April 2010 than prior to the earthquake, and had returned to within one standard deviation of the pre-earthquake values by 12 May 2010, we disfavor response time scales longer than a few days, corresponding to hydraulic diffusivities greater than 10^{-1} m^2 s^{-1}. The return of gas flux to the pre-earthquake values could be a result of (1) recovery of permeability or (2) depletion of the gas source region. Our data do not allow us to discriminate between these mechanisms. Because of the large uncertainty in hydraulic diffusivity, we cannot constrain the depth at which the response occurred.

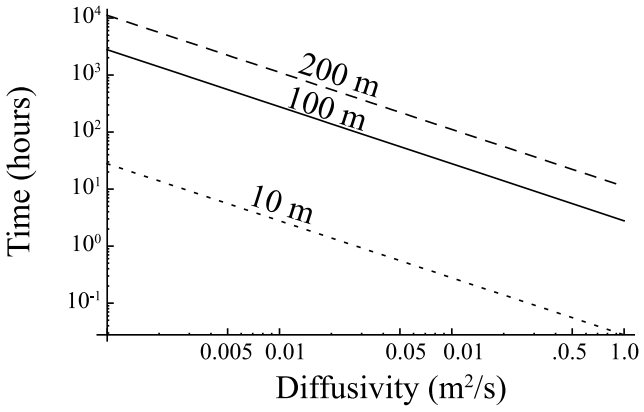

Figure 11. Diffusion time scale as a function of diffusion length scale and diffusivity. We estimate the gas diffusivity in the upper 200 m of the Davis-Schrimpf site as 10^{-3} – 10^0 m^2 s^{-1}. The time scale is at most 10^4 h.

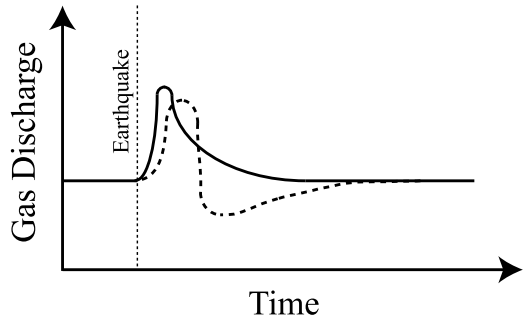

Figure 12. Two hypothetical gas hydrographs for the bubble mobilization mechanism (dashed curve) and permeability enhancement (solid curve) response mechanisms. The bubble mobilization mechanism may cause gas flux to fall below its pre-earthquake value due to depletion of the gas source region.

[37] Lastly, we note that the mobilization of bubbles from an hypothetical bubble source region would deplete that region in bubbles, which might produce a period of lower than average gas discharge, depicted in Figure 12, while the source region was recharged, an effect that would allow us to discriminate between this mechanism and a permeability enhancement mechanism.

6. Conclusions

[38] The measured gas flux at the Davis-Schrimpf mud volcanoes was higher two days after the 4 April 2010 El Mayor-Cucapah earthquake then either one month before or one month after the event. We interpret the observed increase in gas flux as a triggered change in activity. The triggered response is not unexpected based on magnitude-distance-triggering relationships (Figure 9). We considered two seemingly viable triggering mechanisms: bubble mobilization and permeability enhancement. Of these, the latter is more likely to be responsible for the observed response because (1) the time scale associated with the ascent of the small bubbles that would be mobilized by seismic shaking is too long and (2) the time scale associated with the response due to permeability enhancement is consistent with our observations. The rejection of the bubble mobilization mechanism is important because the strain at the Davis-Shrimp mud volcanoes during the El Mayor-Cucapah earthquake was large enough that this mechanism could conceivably have been important. We view the ineffectiveness of the bubble mobilization mechanism in this case study, where mud rheology and shear strain amplitude were favorable, as evidence for the rejection of this mechanism in general. The gas discharge had recovered to within one standard deviation of the pre-earthquake value by 12 May 2010, implying that permeability decreased or that the gas reservoir was depleted during the period of high gas discharge. It would be possible to discriminate between these mechanisms by measuring gas pressure at depth.

[39] Future large earthquakes will provide further opportunities to study mud volcano and hydrologic responses to earthquakes. There have been at least 13 large ($M_W > 6$)

earthquakes in the Imperial and Mexicali Valleys since 1852 [*Anderson and Bodin*, 1987]. Following the next large earthquake, we will make more frequent gas flux measurements and also sample gas with a high temporal frequency with the aim of constraining the source of excess gas or location of increased permeability. We may be able to use the shape of the gas hydrograph (Figure 12) to further constrain the nature of the response mechanism. In this study, we measured only localized gas emission, but there is almost certainly diffuse gas emission from the SSGS and it would be most interesting to see whether it too responds to earthquakes.

[40] **Acknowledgments.** We extend our profuse thanks to David K. Lynch for his generosity in introducing us to the Davis-Schrimpf field site, assisting us with field work on 13 March 2010, and for stimulating conversations about this work and other work being done in this fascinating and beautiful part of California. Benjamin Andrews helped with field work on 13 March 2010. Tim Teague performed the XRD analysis. CILAS Laser Particle Size, Inc. provided us with the grain size measurements. Amanda Thomas assisted with the preparation of Figure 1. We thank Marco Bonini and an anonymous review for comments that improved the quality of the manuscript. This material is based upon work supported under a National Science Foundation Graduate Research Fellowship. This work was further supported by the National Science Foundation under grant EAR-0909701.

References

Adler, P. M., and H. Brenner (1988), Multiphase flow in porous media, *Annu. Rev. Fluid Mech.*, *20*(1), 35–59, doi:10.1146/annurev.fl.20.010188.000343.

Anderson, J., and P. Bodin (1987), Earthquake recurrence models and historical seismicity in the Mexicali-Imperial Valley, *Bull. Seismol. Soc. Am.*, *77*(2), 562–578.

Balderman, M., C. Johnson, D. Miller, and D. Schmidt (1978), The 1852 Fort Yuma earthquake, *Bull. Seismol. Soc. Am.*, *68*(3), 699–710.

Beal, C. (1915), The earthquake in the Imperial Valley, California, June 22, 1915, *Bull. Seismol. Soc. Am.*, *5*(3), 130–149.

Bertani, R. (2005), World geothermal power generation in the period 2001–2005, *Geothermics*, *34*(6), 651–690, doi:10.1016/j.geothermics.2005.09.005.

Bonini, M. (2009a), Mud volcano eruptions and earthquakes in the northern Apennines and Sicily, Italy, *Tectonophysics*, *474*(3-4), 723–735, doi:10.1016/j.tecto.2009.05.018.

Bonini, M. (2009b), Structural controls on a carbon dioxide-driven mud volcano field in the northern Apennines (Pieve Santo Stefano, Italy): Relations with pre-existing steep discontinuities and seismicity, *J. Struct. Geol.*, *31*(1), 44–54, doi:10.1016/j.jsg.2008.10.003.

Brodsky, E., E. Roeloffs, D. Woodcock, I. Gall, and M. Manga (2003), A mechanism for sustained groundwater pressure changes induced by distant earthquakes, *J. Geophys. Res.*, *108*(B8), 2390, doi:10.1029/2002JB002321.

Chigira, M., and K. Tanaka (1997), Structural features and the history of mud volcanoes in Southern Hokkaido, Northern Japan, *J. Geol. Soc. Jpn.*, *103*(8), 781–791.

Clift, R., J. Grace, and M. Weber (Eds.) (1978), *Bubbles, Drops, and Particles*, Academic, New York.

Coussot, P., and J. M. Piau (1994), On the behavior of fine mud suspensions, *Rheol. Acta*, *33*(3), 175–184.

Dubash, N., and I. Frigaard (2004), Conditions for static bubbles in viscoplastic fluids, *Phys. Fluids*, *16*, 4319–4330, doi:10.1063/1.1803391.

Dubash, N., and I. Frigaard (2007), Propagation and stopping of air bubbles in carbopol solutions, *J. Non-Newtonian Fluid Mech.*, *142*(1-3), 123–134, doi:10.1016/j.jnnfm.2006.06.006

Dziewonski, A., T.-A. Chou, and J. Woodhouse (1981), Determination of earthquake source parameters from waveform data for studies of global and regional seismicity, *J. Geophys. Res.*, *86*(B4), 2825–2852.

Elders, W., and J. Sass (1988), The Salton Sea scientific drilling project, *J. Geophys. Res.*, *93*(B11), 12,953–12,968.

Elkhoury, J., E. Brodsky, and D. Agnew (2006), Seismic waves increase permeability, *Nature*, *441*, 1135–1138.

Helgeson, H. C. (1968), Geologic and thermodynamic characteristics of the Salton Sea Geothermal System, *Am. J. Sci.*, *266*(3), 129–166.

Hollander, M., and D. Wolfe (1999), *Nonparametric Statistical Methods*, Wiley, New York.

Hsieh, D. (1961), Theory of rectified diffusion of mass into gas bubbles, *J. Acoust. Soc. Am.*, *33*, 206–215, doi:10.1121/1.1908621.

Hudnut, K., E. Hauksson, D. Given, A. Guarino, S. Hough, K. Hutton, L. Jones, K. Felzer, and B. Dollar (2010), M_w 7.2 El Mayor-Cucapah earthquake, *Tech. Rep.*, Calif. Inst. of Technol., Pasadena.

Husen, S., R. Taylor, R. Smith, and H. Healser (2004), Changes in geyser eruption behavior and remotely triggered seismicity in Yellowstone National Park produced by the 2002 M 7.9 Denali fault earthquake, Alaska, *Geology*, *32*(6), 537–540, doi:10.1130/G20381.1.

Kelley, V. C., and J. L. Soske (1936), Origin of the Salton volcanic domes, Salton Sea, California, *J. Geol.*, *44*(4), 496–509.

King, N., L. Blair, K. Hudnut, and H. Stenner (2010), Report of USGS Activities, El Mayor-Cucapah Earthquake of Sunday, April 4, 2010, *Tech. Rep.*, U.S. Geol. Surv., Reston, Va.

Kopf, A. J. (2002), Significance of mud volcanism, *Rev. Geophys.*, *40*(2), 1005, doi:10.1029/2000RG000093.

Lin, J., and R. Stein (2004), Stress triggering in thrust and subduction earthquakes, and stress interaction between the southern San Andreas and nearby thrust and strike-slip faults, *J. Geophys. Res.*, *109*, B02303, doi:10.1029/2003JB002607.

Liu, W., and M. Manga (2009), Changes in permeability caused by dynamic stresses in fractured sandstone, *Geophys. Res. Lett.*, *36*, L20307, doi:10.1029/2009GL039852.

Lynch, D. K., and K. W. Hudnut (2008), The Wister mud pot lineament: Southeastward extension or abandoned strand of the San Andreas Fault?, *Bull. Seismol. Soc. Am.*, *98*(4), 1720–1729.

Manga, M., and E. Brodsky (2006), Seismic triggering of eruptions in the far field: Volcanoes and geysers, *Annu. Rev. Earth Planet. Sci.*, *34*, 263–291, doi:10.1146/annurev.earth.34.031405.125125.

Manga, M., and H. Stone (1994), Interactions between bubbles in magmas and lavas: Effects of bubble deformation, *J. Volcanol. Geotherm. Res.*, *63*(3-4), 267–279, doi: 10.1016/0377-0273(94)90079-5.

Manga, M., and H. A. Stone (1995), Collective hydrodynamics of deformable drops and bubbles in dilute low reynolds number suspensions, *J. Fluid Mech.*, *300*(1), 231–263, doi:10.1017/S0022112095003673.

Manga, M., M. Brumm, and M. L. Rudolph (2009), Earthquake triggering of mud volcanoes, *J. Mar. Pet. Geol.*, *26*(9), 1785–1798.

Mau, S., G. Rehder, I. G. Arroyo, J. Gossler, and E. Suess (2007), Indications of a link between seismotectonics and CH_4 release from seeps off Costa Rica, *Geochem. Geophys. Geosyst.*, *8*, Q04003, doi:10.1029/2006GC001326.

Mellors, R., D. Kilb, A. Aliyev, A. Gasanov, and G. Yetirmishli (2007), Correlations between earthquakes and large mud volcano eruptions, *J. Geophys. Res.*, *112*, B04304, doi:10.1029/2006JB004489.

Muffler, L., and D. White (1969), Active metamorphism of Upper Cenozoic sediments in the Salton Sea geothermal field and the Salton trough, southeastern California, *Geol. Soc. Am. Bull.*, *80*, 157-182.

Muir-Wood, R., and G. C. P. King (1993), Hydrological signatures of earthquake strain, *J. Geophys. Res.*, *98*(B12), 22,035–22,068.

Obzhirov, A., R. Shakirov, A. Salyuk, E. Suess, N. Biebow, and A. Salomatin (2004), Relations between methane venting, geological structure and seismo-tectonics in the Okhotsk Sea, *Geo Mar. Lett.*, *24*(3), 135–139.

Pridmore, C., S. Brandenburg, T. McCrink, R. Sickler, J. Stewart, and J. Tinsley (2010), Liquefaction and related ground failures in Imperial County, California, caused by the April 4, 2010 El Mayor-Cucapah earthquake, paper presented at 106th Annual Meeting, Am. Assoc. of Pet. Geol., Anaheim, Calif.

Randall, W. (1974), An analysis of the subsurface structure and stratigraphy of the Salton Sea geothermal anomaly, Imperial Valley, California, Ph.D. thesis, Univ. of Calif., Riverside.

Robinson, P., W. Elders, and L. Muffler (1976), Quaternary volcanism in the Salton Sea geothermal field, Imperial Valley, California, *Geol. Soc. Am. Bull.*, *87*, 347–360.

Roeloffs, E. (1996), Poroelastic techniques in the study of earthquake-related hydrologic phenomena, *Adv. Geophys.*, *37*, 136–195.

Rojstaczer, S., and S. Wolf (1992), Permeability changes associated with large earthquakes: An example from Loma Prieta, California, *Geology*, *20*(3), 211–214.

Rojstaczer, S., S. Wolf, and R. Michel (1995), Permeability enhancement in the shallow crust as a cause of earthquake-induced hydrological changes, *Nature*, *373*, 237–239.

Sahagian, D. L., and A. A. Proussevitch (1992), Bubbles in volcanic systems, *Nature*, *359*, 485–485.

Shapiro, S. S., M. B. Wilk, and H. J. Chen (1968), A comparative study of various tests for normality, *J. Am. Stat. Assoc.*, *63*(324), 1343–1372.

Steinberg, G., A. Merzhanov, and A. Steinberg (1982), Geyser process: Its theory, modeling, and field experiment. Part 4. On seismic influence on geyser regime, *Mod. Geol.*, *8*, 79–86.

Steinberg, G., A. Steinberg, and A. Merzhanov (1989), Fluid mechanism of pressure growth in volcanic (magmatic) systems, *Mod. Geol.*, *13*, 257–66.

Sturtevant, B., H. Kanamori, and E. E. Brodsky (1996), Seismic triggering by rectified diffusion in geothermal systems, *J. Geophys. Res.*, *101*, 25,269–25,282, doi:10.1029/96JB02654.

Sturz, A., R. Kamps, and P. Earley (1992), Temporal changes in mud volcanos, Salton Sea geothermal area, in *Water-Rock Interaction*, edited by Y. Kharaka and A. Maest, pp. 1363–1366, Balkema, Rotterdam, Netherlands.

Sumita, I., and M. Manga (2008), Suspension rheology under oscillatory shear and its geophysical implications, *Earth Planet. Sci. Lett.*, *269*, 468–477, doi:10.1016/j.epsl.2008.02.043.

Svensen, H., D. Karlsen, A. Sturz, K. Backer-Owe, D. Banks, and S. Planke (2007), Processes controlling water and hydrocarbon composition in seeps from the Salton Sea Geothermal System, California, USA, *Geology*, *35*(1), 85–88.

Svensen, H., Ø. Hammer, A. Mazzini, N. Onderdonk, S. Polteau, S. Planke, and Y. Podladchikov (2009), Dynamics of hydrothermal seeps from the Salton Sea Geothermal System (California, USA) constrained by temperature monitoring and time series analysis, *J. Geophys. Res.*, B09201, doi:10.1029/2008JB006247.

Toda, S., R. S. Stein, K. Richards-Dinger, and S. Bozkurt (2005), Forecasting the evolution of seismicity in southern California: Animations built on earthquake stress transfer, *J. Geophys. Res.*, *110*, B05S16, doi:10.1029/2004JB003415.

Townley, S., and M. Allen (1939), Descriptive catalog of earthquakes of the Pacific Coast of the United States 1769 to 1928, *Bull. Seismol. Soc. Am.*, *29*(1), 1–297.

Treiman, J., M. Rymer, K. Kendrick, J. Lienkaemper, R. I. Weldon, J. Hernandez, P. Irvine, N. Knepprath, B. Olson, and R. Sickler (2010), Triggered slip in southern California as a result of the April 5, 2010 El Mayor-Cucapah earthquake, paper presented at 106th Annual Meeting, Am. Assoc. of Pet. Geol., Anaheim, Calif.

Walter, T. R., and F. Amelung (2007), Volcanic eruptions following M ≥ 9 megathrust earthquakes: Implications for the Sumatra-Andaman volcanoes, *Geology*, *35*, 539–542, doi:10.1130/FG23429A.1.

Wang, C.-Y. (2007), Liquefaction beyond the near field, *Seismol. Res. Lett.*, *78*(5), 512–517, doi:10.1785/gssrl.78.5.512.

Wang, C.-Y., and M. Manga (2010), Hydrologic responses to earthquakes and a general metric, *Geofluids*, *10*(1-2), 206–216.

Wang, C.-Y., L.-H. Cheng, C.-V. Chin, and S.-B. Yu (2001), Coseismic hydrologic response of an alluvial fan to the 1999 Chi-Chi earthquake, Taiwan, *Geology*, *29*(9), 831–834.

Wang, C.-Y., D. Dreger, C.-H. Wang, D. Mayeri, and J. Berryman (2003), Field relations among coseismic ground motion, water level change and liquefaction for the 1999 Chi-Chi (M_w = 7.5) earthquake, Taiwan, *Geophys. Res. Lett.*, *30*(17), 1890, doi:10.1029/2003GL017601.

Wang, C.-Y., M. Manga, D. Dreger, and A. Wong (2004a), Streamflow increase due to rupturing of hydrothermal reservoirs: Evidence from the 2003 San Simeon, California, earthquake, *Geophys. Res. Lett.*, *31*, L10502, doi:10.1029/2004GL020124.

Wang, C.-Y., C.-H. Wang, and M. Manga (2004b), Coseismic release of water from mountains: Evidence from the 1999 (Mw 7.5) Chi-Chi, Taiwan, earthquake, *Geology*, *32*(9), 769–772.

Wells, D. L., and K. J. Coppersmith (1994), New empirical relationships among magnitude, rupture length, rupture width, rupture area, and surface displacement, *Bull. Seismol. Soc. Am.*, *84*(4), 974–1002.

Williams, A. E., and M. A. McKibben (1989), A brine interface in the Salton Sea Geothermal System, California: Fluid geochemical and isotopic characteristics, *Geochim. Cosmochim. Acta*, *53*(8), 1905–1920, doi:10.1016/0016-7037(89)90312-8.

Youd, T., B. H. A. J., and J. Proctor (2004), Geotechnical logs and data from permanently instrumented field sites: Garner Valley Down Hole Array(GVDA) and Wildlife Liquefaction Array (WLA), *Tech. Rep.*, Network for Earthquake Eng. Simul., West Lafayette, Indiana.

Younker, L. W., P. W. Kasameyer, and J. D. Tewhey (1982), Geological, geophysical, and thermal characteristics of the Salton Sea geothermal field, California, *J. Volc. Geothermal Res.*, *12*(3-4), 221–258, doi:10.1016/0377-0273(82)90028-2.

M. Manga and M. L. Rudolph, Department of Earth and Planetary Science, University of California, 307 McCone Hall, Berkeley, CA 94720, USA. (max@seismo.berkeley.edu)